non-ambient crystallography

Temperature- and pressure-dependent structural study of {Fe(pmd)$_2$[Ag(CN)$_2$]$_2$}$_n$ spin-crossover compound by neutron Laue diffraction

José Alberto Rodríguez-Velamazán,[a,b]* Laura Cañadillas-Delgado,[a,c] Miguel Castro,[a] Garry J. McIntyre[b]‡ and José Antonio Real[d]

[a]Instituto de Ciencia de Materiales de Aragón, CSIC-Universidad de Zaragoza, C/Pedro Cerbuna 12, E-50009 Zaragoza, Spain, [b]Institut Laue–Langevin, 6 rue Jules Horowitz, BP 156, 38042 Grenoble, France, [c]Centro Universitario de la Defensa de Zaragoza, Ctra Huesca s/n, 50090 Zaragoza, Spain, and [d]Instituto de Ciencia Molecular (ICMol), Universidad de Valencia, Paterna, E-46980 Valencia, Spain

‡ Present address:, Australian Nuclear Science and Technology Organisation, Lucas Heights, NSW 2234, Australia.

Correspondence e-mail: jarv@unizar.es

The effect of pressure (up to 0.17 GPa) on the spin-crossover compound {Fe(pmd)$_2$[Ag(CN)$_2$]$_2$}$_n$ [orthorhombic isomer (II), pmd = pyrimidine] has been investigated by temperature- and pressure-dependent neutron Laue diffraction and magneto-metry. The cooperative high-spin ↔ low-spin transition, centred at *ca* 180 K at ambient pressure, is shifted to higher temperatures as pressure is applied, showing a moderate sensitivity of the compound to pressure, since the spin transition is displaced by *ca* 140 K GPa^{-1}. The space-group symmetry (orthorhombic *Pccn*) remains unchanged over the pressure–temperature (P–T) range studied. The main structural consequence of the high-spin to low-spin transition is the contraction of the distorted octahedral [FeN$_6$] chromophores, being more marked in the axial positions (occupied by the pmd units), than in the equatorial positions (occupied by four [Ag(CN)$_2$]$^-$ bridging ligands).

1. Introduction

One of the challenges in the area of molecular magnetism is the search for switchable magnetic materials, which are potential candidates for applications in information storage devices, molecular switches and sensors. Potentially interesting materials are those that display bistability between two or more different magnetic states. Spin-crossover (SCO) compounds, most frequently Fe^{II} complexes, are the paradigmatic example of molecular switching in the solid state. In these compounds, the interconversion between low-spin (LS) and high-spin (HS) states can be triggered by different external parameters, such as temperature, pressure, external electric and magnetic field, light irradiation, and even by the action of an analyte (Linert & Verdaguer, 2003; Gütlich & Goodwin, 2004a; Gütlich *et al.*, 2013).

The spin-crossover phenomenon is well understood on the basis of ligand-field theory (Hauser, 2004). SCO compounds show a LS ground state at low temperatures characterized by high ligand-field strength and a HS state at high temperatures with low ligand-field strength. The LS-to-HS transition is typically accompanied by a substantial elongation of the metal–ligand bond lengths and, in fact, the dependence of the ligand field strength on the metal–ligand distance may be considered the quantum mechanical driving force for the SCO phenomenon. A major part of the known spin-crossover complexes contain Fe^{II} in a $3d^6$ electronic configuration and a N$_6$ first coordination sphere. For these compounds, the change in Fe—N distances from the LS to the HS state is typically ∼ 0.2 Å. The structural characteristics of the coordination sphere around the central ions are crucial to understand the properties of these materials.

The bistability is accomplished when the cooperative behaviour between SCO metal centres gives rise to discontinuous spin transitions with hysteresis. One of the most successful routes for the cooperativity enhancement is the synthesis of SCO polymeric compounds derived from the well known Hofmann clathrates, in which the metal centres are linked with cyanometalate complexes into extended or polymeric structures with different dimensionalities and topologies. Since the description of the first compound of this type, $Fe(py)_2[Ni(CN)_4]$ (py = pyridine; Kitazawa *et al.*, 1996), this approach has been extensively explored (see for example Niel *et al.*, 2001; Papanikolaou *et al.*, 2006; Rodríguez-Velamazán *et al.*, 2007, 2010; Ohkoshi *et al.*, 2011; Muñoz & Real, 2011), with derivations like the substitution of the cyanometallate anion for new types of metalloligand building blocks with similar structural functionality (Muñoz-Lara *et al.*, 2012).

Following this approach, the combination of iron(II) ions, $[M^I(CN)_2]^-$ groups and pyrimidine ligands has produced SCO polymers with different topologies and interesting thermal-, pressure- and light-induced properties (Niel, Galet *et al.*, 2003; Niel, Thompson *et al.*, 2003 Niel *et al.*, 2005; Galet, Gaspar *et al.*, 2005; Galet, Muñoz *et al.*, 2005; Agustí *et al.*, 2008). $\{Fe(pmd)_2[Ag(CN)_2]_2\}_n$ was first reported in 2005 (Galet, Muñoz *et al.*, 2005). It crystallizes in two architectural isomers with different structures and properties: isomer (I) remains in the HS state over the whole temperature range, while isomer (II) displays a cooperative spin transition centred at *ca* 184 K. The orthorhombic *Pccn* space-group symmetry of isomer (II) remains the same in both the HS and the LS states at ambient pressure, with the following unit cell at 250 K [150 K]: $a = 15.7700\ (2)$ [14.8950 (2)], $b = 8.2980\ (4)$ [8.1580 (4)], $c = 13.4180\ (6)$ Å [13.3480 (5) Å], $V = 1755.87\ (14)$ Å^3 [1621.96 (10) Å^3], $Z = 4$. The structure (Fig. 1) can be depicted as (4,4)-layers, where each iron(II) atom is linked to four $[Ag(CN)_2]^-$ anions which run parallel to the *ac* plane. These planes are connected through the pmd ligands to the adjacent ones, constructing the final three-dimensional structure (Galet, Muñoz *et al.*, 2005).

The main effect of pressure on SCO materials is the stabilization of the LS state, thus shifting the transition to higher temperatures. This is due to the mentioned noticeable volume reduction related to the change of the metal–ligand bond lengths between the HS and LS states. The applied pressure increases the difference between the zero-point energies of the LS and HS states by $P\Delta V$ and stabilizes the state with less volume. Other secondary effects of pressure are, for example, changes in the width of hysteresis loops, or increasing residual fractions of LS and HS species which do not undergo the spin transition (Gütlich & Goodwin, 2004*b*; Gutlich *et al.*, 2005; Ksenofontov *et al.*, 2004), although several deviations from this behaviour have been observed, generally attributed to a complex structural P–T phase diagram (Gutlich *et al.*, 2005; Legrand *et al.*, 2013). Most of the studies of SCO compounds under pressure make use of spectroscopic measurements or magnetometry (Jeftić *et al.*, 1996, 1997; Jeftić & Hauser, 1997; Ksenofontov *et al.*, 2004; Molnár *et al.*, 2003, 2004; Shepherd, Bartual-Murgui *et al.*, 2011). To gain a deeper insight into such

pressure effects, structure determinations under applied pressure and at variable temperature are highly desirable. However, reported studies of this type are not frequent
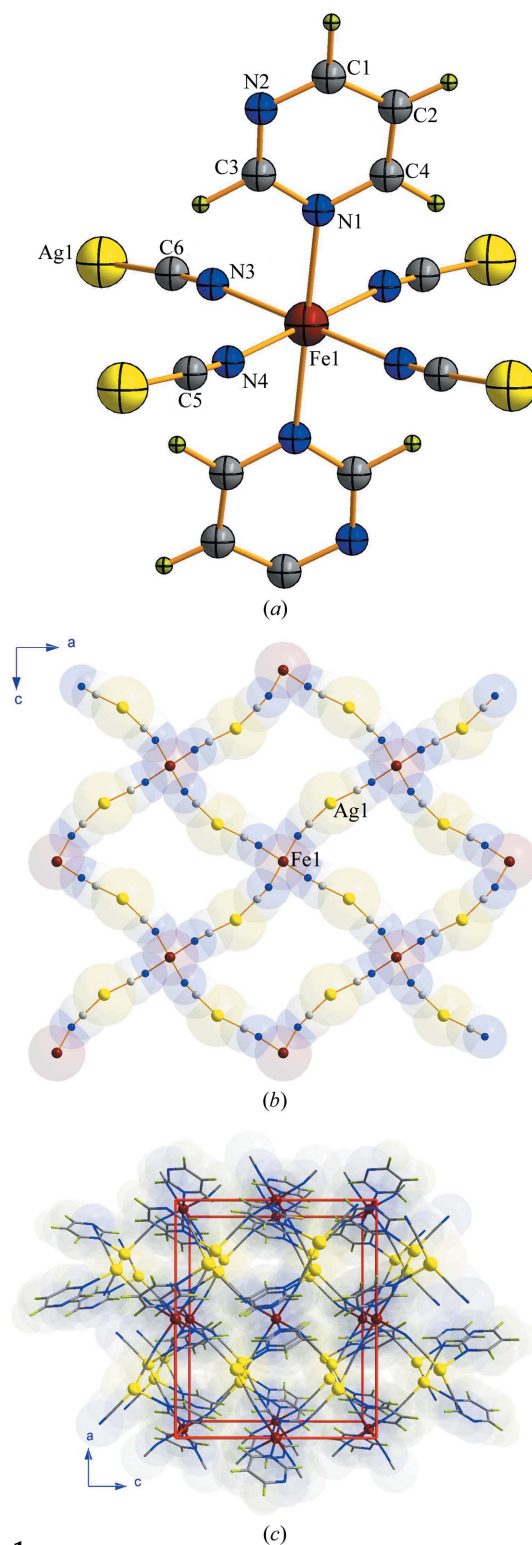
Figure 1
Views of the structure of $\{Fe(pmd)_2[Ag(CN)_2]_2\}_n$ [isomer (II)] as reported by Galet, Muñoz *et al.* (2005) from X-ray measurements at 250 K and at ambient pressure showing (*a*) the atom numbering of the structure, (*b*) the layers formed by iron(II) and $[Ag(CN)_2]^-$ ions, and (*c*) the crystal packing of the layers.

Table 1
Experimental details.

Crystal data	
Chemical formula	$C_{12}H_8Ag_2FeN_8$
M_r	535.83
Crystal system, space group	Orthorhombic, $Pccn$
a, b, c (Å)†	15.7700 (2), 8.2980 (4), 13.4180 (5)
V (Å^3)†	1755.87 (14)
Z	4
Radiation type	Neutron, λ = 0.90-3.00 Å‡
Crystal size (mm^3)	$1.0 \times 0.6 \times 0.5$
Data collection	
Diffractometer	ILL-VIVALDI Laue single-crystal diffractometer
Absorption correction	–
H-atom treatment	All H-atom parameters refined

Measurement	1	2	3	4	5	6	7	8	9	10	11	12	13
T (K)	150	187	210	240	260	200	250	280	250	220	260	280	290
P (GPa)	0.101	0.111	0.106	0.106	0.102	0.123	0.126	0.125	0.143	0.160	0.156	0.163	0.181
Measured reflns	7581	5504	2295	3616	5945	4785	2764	3564	2910	3553	5638	3459	5485
Independent reflns	1543	1210	686	788	1291	991	661	797	772	973	1069	782	1068
Observed $[I > 2\sigma(I)]$ reflns	1236	943	510	641	978	735	600	674	618	743	885	641	860
R_{int}	0.197	0.321	0.259	0.267	0.185	0.366	0.378	0.300	0.242	0.357	0.221	0.352	0.227
$R[F^2 > 2\sigma(F^2)]$	0.083	0.166	0.1581	0.128	0.079	0.172	0.192	0.169	0.155	0.167	0.100	0.172	0.114
$wR(F^2)$,	0.149	0.281	0.2608	0.207	0.155	0.337	0.346	0.259	0.194	0.307	0.161	0.293	0.168
S	1.24	1.35	1.38	1.28	1.16	1.36	1.54	1.51	1.45	1.40	1.29	1.42	1.30

Computer programs: *LAUEGEN* (Campbell *et al.*, 1998), *ARGONNE BOXES* (Wilkinson *et al.*, 1988), *LAUENORM* (Campbell *et al.*, 1986), *SHELXL97* (Sheldrick, 2008). † X-ray values at ambient pressure and temperature (from Galet, Muñoz *et al.*, 2005) ‡ Wavelength bandwidth effectively used after data reduction.

(Granier *et al.*, 1993; Guionneau *et al.*, 2001, 2005; Shepherd, Bonnet *et al.*, 2011; Shepherd, Palamarciuc *et al.*, 2012; Shepherd, Rosa *et al.*, 2012), probably due to the well known experimental difficulties involving pressure- and temperature-dependent crystal-structure determinations. In the range of moderate pressures in which most of the pressure effects in SCO compounds are observed – up to 2 GPa – neutron diffraction is a suitable but very rarely exploited (Legrand *et al.*, 2008, 2013; Lemée-Cailleau *et al.*, 2007) alternative to X-rays. The penetration power of neutrons allows the use, in combination with standard cryostats, of high-volume pressure cells like the Ti–Zr gas ones (Klotz, 2012), which allow continuous change of pressure and perfect hydrostaticity and isotropy. For single-crystal studies in particular, these cells have the advantage of a very large aperture (full access in the horizontal plane and *ca* $\pm 50°$ out of the plane; McIntyre *et al.*, 2005). The acceptable sample volumes are limited, but the Laue technique allows sample volumes several orders of magnitude smaller than is usual for single-crystal neutron diffraction (Wilkinson *et al.*, 2002).

Here the structural properties of the spin-transition compound $\{Fe(pmd)_2[Ag(CN)_2]_2\}_n$ [isomer (II)] are investigated using single-crystal neutron diffraction at different temperatures and under pressures up to 0.17 GPa, and compared with temperature- and pressure-dependent magnetometry results, with the aim of correlating the spin-

transition properties to the structural variations under pressure.

2. Experimental

2.1. Synthesis

The synthesis of $\{Fe(pmd)_2[Ag(CN)_2]_2\}_n$ [isomer (II)] was performed according to the previously reported procedure (Galet, Muñoz *et al.*, 2005) by slow diffusion in a H-shaped vessel of an aqueous solution containing a mixture of stoichiometric amounts of pmd and $Fe(BF_4)_2\cdot6H_2O$ on one side, and an aqueous solution of $K[Ag(CN)_2]$ on the other side. Crystals of isomers (I) and (II) are obtained in the same reaction, and those of isomer (II) selected by ocular inspection.

2.2. Magnetic susceptibility measurements at variable pressure and temperature

The magnetic susceptibility *versus* temperature measurements under hydrostatic pressure were performed on a Quantum Design MPMS2 SQUID magnetometer between 5 and 300 K in an applied external field of 1 T. A microcrystalline powder of $\{Fe(pmd)_2[Ag(CN)_2]_2\}_n$ [isomer (II)] was loaded into the hydrostatic pressure cell made of hardened beryllium bronze with silicone oil as the pressure-

transmitting medium. The cell operates in the pressure range 10^5 Pa $< P < 1.2$ GPa (accuracy $\simeq \pm 0.025$ GPa). Cylindrically shaped powder sample holders of 1 mm diameter and 5–7 mm length were used. The pressure was determined using the pressure dependence of the superconducting transition temperature of a built-in pressure sensor made of high-purity tin (Baran *et al.*, 1995). The data were corrected for the magnetization of the sample holder and for diamagnetic contributions, estimated from Pascal's constants.

2.3. Single-crystal neutron diffraction at variable pressure and temperature

The temperature- and pressure-dependent single-crystal neutron diffraction experiments (Table 1) were carried out at the high-flux reactor of the Institut Laue–Langevin (ILL, Grenoble), using the very-intense vertical-axis Laue diffractometer (*VIVALDI*; Wilkinson *et al.*, 2002; McIntyre *et al.*, 2005, 2006) Crystals of the title compound are stable at room temperature. A single crystal with approximate dimensions $1 \times 0.6 \times 0.5$ mm was mounted on a vanadium pin. The pin was placed in a Ti–Zr continuously loaded He-gas pressure cell (Klotz, 2012) which in turn was inserted in a standard orange cryostat. The high-pressure medium was helium gas, which assures a perfect hydrostaticity and isotropy of the applied pressure at all measured temperatures down to 150 K. An external automated compressor maintained constant pressure even when temperature was changed (accuracy in pressure $\simeq \pm 0.001$ GPa, given by the manometer of the compressor).

Data collections were completed at 13 different points in the P–T space. Each collection consisted of 6 Laue diffraction patterns, each accumulated typically for 90 to 120 min, at intervals of $20°$ in φ (rotation of the crystal along a vertical axis perpendicular to the incident beam), from -15 to $85°$. The intensities were indexed and processed using the program *LAUEGEN* (Campbell, 1995; Campbell *et al.*, 1998) and integration was performed using the program *ARGONNE BOXES* (Wilkinson *et al.*, 1988), which uses a two-dimensional version of the minimum $\sigma(I)/I$ algorithm (Lehmann & Larsen, 1974). The reflections were normalized to a constant incident wavelength using the program *LAUENORM* (Campbell *et al.*, 1986). Subsequent calculations for structure determination were carried out using the *SHELX* package (Sheldrick, 2008). Basic models derived from the ambient pressure phase were used as a starting point for refinement of structural parameters against high-pressure data on F^2. All atoms, including hydrogen, were refined anisotropically. No constraints or restraints were applied, except for the H4 and C4 atoms in data set 3, that have been constrained to have the same anisotropic displacement parameters using an EADP command. The final geometrical calculations and the graphical manipulations were carried out with *PARST95* (Nardelli, 1995), *PLATON* (Spek, 2009) and *DIAMOND* (Brandenburg, 1999) programs.

The Laue diffractometer VIVALDI uses a thermal-neutron white beam with a large wavelength bandwidth from 0.80 to 5.20 Å. After an *hkl* assignment, orientation refinement and intensity integration for each peak observed on the detector, intensity normalization to a common incident wavelength was conducted in order to produce a data set suitable for structure analysis. The normalization is based on the redundant measurement of Bragg reflections and their symmetry equivalents for different sample orientations and therefore for different wavelengths that should give the same intensity once the wavelength distribution of the incident beam is accounted for. The wavelength distribution is modeled by a high-order polynomial, which is well adapted when the incident beam is not too perturbed from its source to the sample. In the case of *VIVALDI*, the presence of several monochromators upstream disrupts strongly the wavelength distribution with sharp intensity fluctuations of the order of ± 25%, producing internal R-factors that are usually in the range 15–25%. Moreover, in our case the application of pressure and temperature cycling degrades the data quality.

A direct consequence of this fact, if the usual indicators are considered, is that data quality is lower than that produced by monochromatic instruments. However, the crystal-structure refinement based on Laue data is not a 'standard' technique and the final values of R_{int}, $R(F^2)$ and $wR(F^2)$ cannot be easily compared with those obtained from monochromatic instruments; it should be noted that all spots coming from superposed harmonics as well as overlapping spots are rejected. Nevertheless, such data give access to structures with a reasonably good description of atomic positions, including H atoms which are barely visible with X-ray diffraction measurements.

3. Results and discussion

3.1. Magnetic behaviour under pressure

The dependence of the $\chi_M T$ product with temperature (where χ_M is the molar magnetic susceptibility and T is the
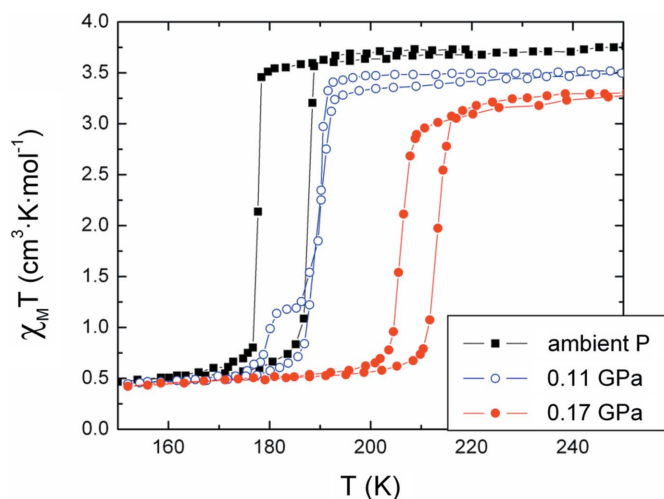
Figure 2
$\chi_M T$ versus T plots for $\{Fe(pmd)_2[Ag(CN)_2]_2\}_n$ [isomer (II)] at ambient pressure (closed squares), 0.11 GPa (open circles), 0.17 GPa (closed circles)

Table 2
Main crystallographic parameters obtained from the neutron Laue diffraction study, and values reported by Galet, Muñoz, Gaspar & Real (2005).

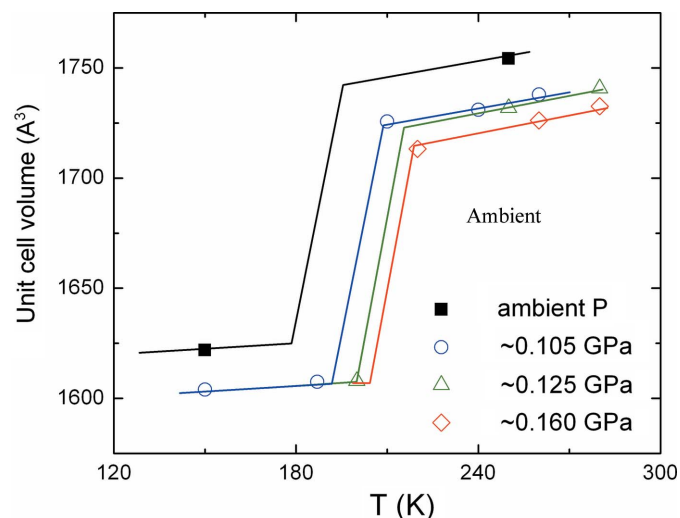| Data collection No.	P (GPa)	T (K)	a (Å)	b (Å)	c (Å)	V (Å³)	Fe1—N4 (Å)	Fe1—N3 (Å)	Fe1—N1 (Å)	Mean Fe—N distance (Å)	Spin state
1	0.101	150	14.895 (3)	8.106 (3)	13.285 (3)	1604.0 (8)	1.926 (2)	1.934 (2)	1.998 (2)	1.953 (2)	LS
2	0.111	187	14.895 (3)	8.122 (3)	13.288 (3)	1607.5 (8)	1.932 (5)	1.939 (4)	1.992 (6)	1.954 (6)	LS
3	0.106	210	15.782 (3)	8.218 (3)	13.305 (3)	1725.6 (8)	2.130 (10)	2.145 (9)	2.252 (10)	2.176 (10)	HS
4	0.106	240	15.782 (3)	8.235 (3)	13.319 (3)	1731.0 (8)	2.125 (6)	2.135 (5)	2.216 (5)	2.159 (6)	HS
5	0.102	260	15.780 (3)	8.250 (3)	13.350 (3)	1738.0 (8)	2.120 (2)	2.142 (2)	2.225 (2)	2.162 (2)	HS
6	0.123	200	14.895 (3)	8.125 (3)	13.286 (3)	1607.9 (8)	1.934 (6)	1.923 (6)	1.998 (8)	1.952 (8)	LS
7	0.126	250	15.782 (3)	8.235 (3)	13.325 (3)	1731.8 (8)	2.128 (11)	2.119 (10)	2.205 (11)	2.151 (11)	HS
8	0.125	280	15.782 (3)	8.262 (3)	13.350 (3)	1740.7 (8)	2.124 (7)	2.138 (6)	2.222 (7)	2.161 (7)	HS
9	0.143	250	15.782 (3)	8.229 (3)	13.304 (3)	1727.8 (8)	2.130 (7)	2.129 (6)	2.217 (7)	2.159 (7)	HS
10	0.160	220	15.780 (3)	8.200 (3)	13.240 (3)	1713.2 (8)	2.118 (7)	2.123 (6)	2.204 (7)	2.148 (7)	HS
11	0.156	260	15.782 (2)	8.225 (2)	13.298 (2)	1726.2 (4)	2.120 (3)	2.141 (3)	2.221 (3)	2.160 (3)	HS
12	0.163	280	15.782 (3)	8.242 (3)	13.320 (3)	1732.6 (8)	2.132 (9)	2.132 (8)	2.214 (9)	2.159 (9)	HS
13	0.181	290	15.782 (2)	8.243 (2)	13.310 (2)	1731.5 (4)	2.121 (3)	2.142 (3)	2.217 (3)	2.160 (3)	HS
Galet, Muñoz *et al.* (2005)	10^{-4}	150	14.8950 (2)	8.1580 (4)	13.3480 (5)	1622.0 (1)	1.946 (2)†	1.932 (2)	2.002 (2)	1.960 (2)	LS
	10^{-4}	250	15.7700 (2)	8.2980 (4)	13.4180 (6)	1755.9 (1)	2.154 (2)†	2.133 (2)	2.230 (2)	2.172 (2)	HS

† N4 in our labelling corresponds to N2 in the labelling of Galet, Muñoz *et al.* (2005).

temperature) has been recorded at ambient pressure, at 0.11 and at 0.17 GPa (Fig. 2). At ambient pressure, the sample shows similar behaviour to that previously reported (Galet, Muñoz *et al.*, 2005): a first-order spin transition centred at *ca* 183 K. The main differences are a wider hysteresis (*ca* 10 K) and a higher content of residual HS molar fraction at low temperatures (*ca* 0.45 cm³ K mol⁻¹, *ca* 12%). This amount of residual HS centres is common and typically associated with the presence of a larger number of defects in the crystals.

At 0.11 GPa, $\chi_M T$ reaches a value of 3.5 cm³ K mol⁻¹ at 250 K, in the range expected for iron(II) in the HS state but

Figure 3
Volume variation as a function of temperature for different selected pressures as estimated by Laue neutron diffraction (open symbols), together with the previously reported values obtained by X-rays at ambient pressure (Galet, Muñoz *et al.*, 2005; full squares). The lines are guides to the eye and the error bars are approximately the size of the symbols. Note that the white-beam Laue technique does not allow determining the absolute unit-cell volume, but it will show when there is a change due to changes in the ratios between unit-cell dimensions.

slightly lower than at ambient pressure, indicating an increase of the residual fraction of LS species not undergoing the spin transition, a common observation in SCO compounds under pressure (Gütlich & Goodwin, 2004b; Ksenofontov *et al.*, 2004). This value remains approximately constant on cooling down to *ca* 190 K, then decreases abruptly to *ca* 1.2 cm³ K mol⁻¹ at 185 K, describing a step of 4 K, and finally drops again to *ca* 0.45 cm³ K mol⁻¹ below *ca* 165 K. On heating, the low-temperature value of *ca* 0.45 cm³ K mol⁻¹ keeps almost constant up to *ca* 183 K, and then increases steeply, matching approximately the cooling curve above 190 K. This describes an uncommon spin transition which is two-step on cooling and one-step on heating, with a hysteresis of *ca* 7 K in the low-temperature step. This can be due to slow kinetics taking place in the cooling mode, which affords a mixture of two phases: one metastable minor phase whose magnetic behaviour resembles that of the precursor phase at ambient pressure and a major new phase that does not display significant thermal hysteresis. In fact, this hypothesis is supported by the observation of a phase coexistence evolving with time in some neutron Laue diffraction patterns collected close to the spin transition (see the supporting information[1]).

Finally, at 0.17 GPa the transition is markedly shifted to higher temperatures. Furthermore, the cooperative nature of the spin transition reappears displaying a hysteresis loop 7 K wide centred at around 210 K. This hysteresis is 3 K narrower than at 10^{-4} GPa (ambient pressure), a fact that is predicted by the well known regular solutions model (Slichter & Drickamer, 1972). At this pressure the $\chi_M T$ value is *ca* 3.3 cm³ K mol⁻¹ in the temperature range 215–250 K and denotes an increase of residual LS centres coexisting with the thermodynamically stable HS state. The opening of the hysteresis loop with respect to the spin transition at 0.11 GPa

---

[1] Supporting information for this paper is available from the IUCr electronic archives (Reference: XK5013).

is an uncommon event, but different examples of a similar behaviour have been previously reported (Gutlich *et al.*, 2005; Legrand *et al.*, 2013), and in particular this is the case for the closely related compound {Fe(pmd)(H$_2$O)[Ag(CN)$_2$]$_2$}·H$_2$O (Galet, Gaspar *et al.*, 2005).

3.2. Structural analysis by single-crystal neutron diffraction under applied pressure

The main crystallographic parameters obtained from the neutron Laue diffraction study are listed in Table 2. The space-group symmetry (orthorhombic *Pccn*) remains unchanged over the *P–T* range studied. Since only the ratios between unit-cell dimensions can be determined in the white-beam Laue technique, we have considered as a starting point the reported values obtained by X-ray diffraction at ambient pressure (Galet, Muñoz *et al.*, 2005) and refined only two out of the three cell parameters at a time. Typically we started refining *b* and *c* and then we fixed one of them and refined *a*. Despite this limitation, the obtained unit-cell volumes allow us to identify the LS or HS state of the crystal in the different *P–T* points measured (Fig. 3), with the LS state being characterized by a marked contraction in volume.

A more accurate picture is obtained by analyzing the changes in the [FeN$_6$] octahedron (Fig. 4) within the limits of the uncertainty in the absolute unit-cell volumes. The LS state is characterized by a mean Fe—N distance of *ca* 1.95 Å, while in the HS state this value is *ca* 2.16 Å. At ambient pressure (Galet, Muñoz *et al.*, 2005) the axial Fe—N distances, occupied by the pmd units, are larger than the equatorial ones, occupied by the cyanide groups of the [Ag(CN)$_2$]$^-$ anions [Fe—N1 = 2.230 (2) Å at 250 K and 2.002 (2) Å at 150 K; Fe—N3 = 2.133 (2) Å and Fe—N4 = 2.154 (2) Å at 250 K and 1.932 (2) and 1.946 (2) Å at 150 K, respectively],[2] a characteristic which is conserved under applied pressure (Table 2). In a similar way as observed in the temperature-induced spin transition at ambient pressure, the distorted coordination octahedra show a more marked contraction in the apical positions. The Fe1—N1 distance (apical) decreases 10.2% at ambient pressure, while the equatorial Fe1—N3 and Fe1—N4 distances are reduced by 9.4 and 9.6%, respectively. Similarly, when the transition takes place under applied pressure, it results in a reduction of 10.1% in the apical distance and 9.5% for Fe1—N3 and Fe1—N4 distances when we compare the data taken at 0.12 GPa and at 280 and 200 K, respectively (data collections 6 and 8), which correspond to a temperature variation comparable to that of the data at ambient pressure (Galet, Muñoz *et al.*, 2005).

With the magnetic and structural measurements we can depict the *P–T* phase diagram of {Fe(pmd)$_2$[Ag(CN)$_2$]$_2$}$_n$ [isomer (II)] in the studied moderate-pressure region (Fig. 5), which is characterized by a moderate linear increase of the transition temperature as pressure increases, with a slope of 140 K GPa^{-1}. In the mean-field approach, the pressure dependence of the transition temperature is expected to be linear with a slope given by $\Delta V_{\mathrm{HL}}/\Delta S_{\mathrm{HL}}$, with ΔV_{HL} the

[2] Note that N4 in our labelling corresponds to N2 in the labelling of Galet, Muñoz *et al.* (2005).
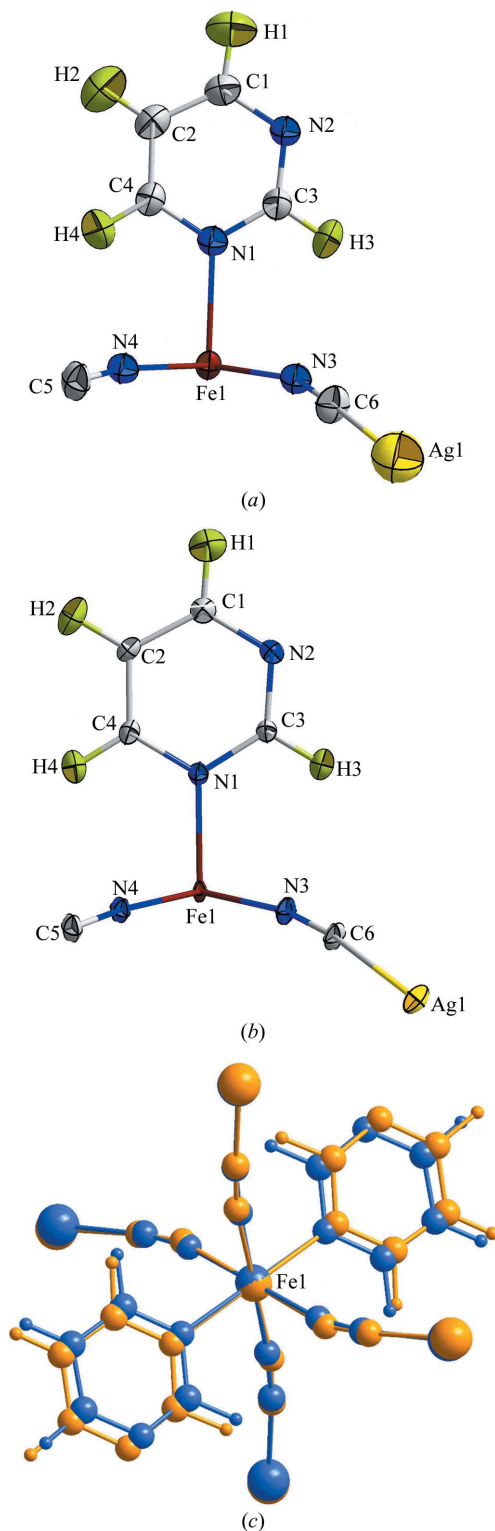
Figure 4
ORTEP representations of the asymmetric unit of {Fe(pmd)$_2$-[Ag(CN)$_2$]$_2$}$_n$ [isomer (II)] corresponding to the structure refinements at 0.10 GPa, in the HS state at 260 K (*a*) and in the LS state at 150 K (*b*). Displacement ellipsoids are presented at 50% probability. (*c*) View of the superposition of the Fe1 environments before and after the transition, where the HS (0.12 GPa, 250 K) and LS (0.12 GPa, 200 K) structures have been represented in orange and blue, respectively.

non-ambient crystallography
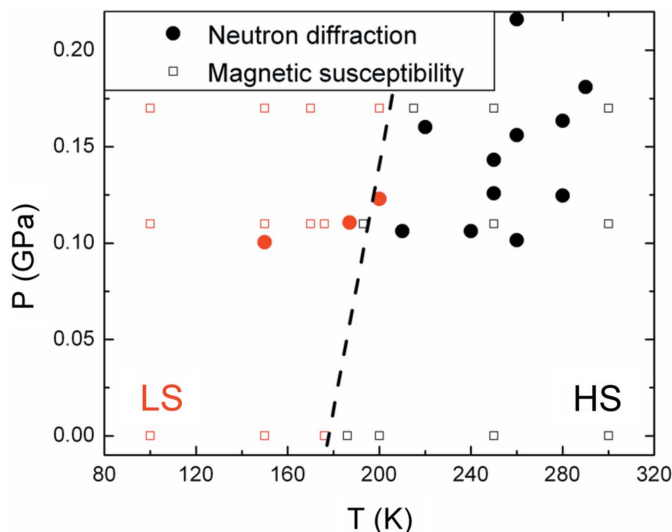
Figure 5
Pressure–temperature phase diagram of {Fe(pmd)$_2$[Ag(CN)$_2$]$_2$}$_n$ [isomer (II)] derived from magnetic susceptibility measurements (open squares) and structural data (full circles). The LS and HS states are denoted by red and black markers, respectively. The dashed line marks the spin transition region.

volume change in the transition and ΔS_{HL} its entropy content (Ksenofontov *et al.*, 2004). Considering the values of ΔV_{HL} (133.9 Å^3) and ΔS_{HL} (64 J mol^{-1} K^{-1}) at ambient pressure (Galet, Muñoz *et al.*, 2005), the theoretical slope will be 315 K GPa^{-1}, *ca* twice that observed. This deviation is nevertheless not surprising, as several SCO systems have been reported in which the effect of pressure on the SCO behaviour cannot be adequately described in terms of this theory (Ksenofontov *et al.*, 2004). Moreover, similar behaviour has been observed in the low-pressure region for the closely related compound {Fe(pmd)$_2$[Cu(CN)$_2$]$_2$}$_n$ (Agustí *et al.*, 2008), where a very weak pressure dependence has been observed up to 0.22 GPa, followed at higher pressures by an apparent linear increase of the transition temperature at a rate which almost doubles the mean-field prediction.

4. Conclusions

Reported studies concerning structure determinations of spin-crossover systems under applied pressure are rather scarce (and even more so when combined with variable temperature), although these are crucial to explain in depth the effects of pressure in the spin transition. The present work shows the possibilities of neutron Laue diffraction for structural investigations under moderate pressure of spin-crossover compounds and other similar systems. The compound {Fe(pmd)$_2$[Ag(CN)$_2$]$_2$}$_n$ [isomer (II), pmd = pyrimidine] has been investigated by temperature- and pressure-dependent neutron Laue diffraction and the results correlated with magnetometry data to describe the P–T phase diagram of this compound. A shift of the spin transition to higher temperatures is observed when pressure is applied. The transition is characterized by a contraction of the [FeN$_6$] octahedra, more

noticeably in the axial positions, with no change in the orthorhombic space-group symmetry (*Pccn*).

References

Agustí, G., Thompson, A. L., Gaspar, A. B., Muñoz, M. C., Goeta, A. E., Rodríguez-Velamazán, J. A., Castro, M., Burriel, R. & Real, J. A. (2008). *Dalton Trans.* pp. 642–649
Baran, M., Dyakonov, V., Gładczuk, L., Levchenko, G., Piechota, S. & Szymczak, H. (1995). *Physica C*, **241**, 383–388.
Brandenburg, K. (1999). *DIAMOND.* Crystal Impact GbR, Bonn, Germany.
Campbell, J. W. (1995). *J. Appl. Cryst.* **28**, 228–236.
Campbell, J. W., Habash, J., Helliwell, J. R. & Moffat, K. (1986). *Info. Quart. Prot. Crystallogr.* **18**, 23–31.
Campbell, J. W., Hao, Q., Harding, M. M., Nguti, N. D. & Wilkinson, C. (1998). *J. Appl. Cryst.* **31**, 496–502.
Galet, A., Gaspar, A. B., Muñoz, M. C., Bukin, G. V., Levchenko, G. & Real, J. A. (2005). *Adv. Mater.* **17**, 2949–2953.
Galet, A., Muñoz, M. C., Gaspar, A. B. & Real, J. A. (2005). *Inorg. Chem.* **44**, 8749–8755.
Granier, T., Gallois, B., Gaultier, J., Real, J. A. & Zarembowitch, J. (1993). *Inorg. Chem.* **32**, 5305–5312.
Guionneau, P., Marchivie, M., Garcia, Y., Howard, J. A. K. & Chasseau, D. (2005). *Phys. Rev. B*, **72**, 214408.
Guionneau, P., Brigouleix, C., Barrans, Y., Goeta, A. E., Létard, J.-F., Howard, J. A. K., Gaultier, J. & Chasseau, D. (2001). *C. R. Acad. Sci. Paris*, **4**, 161–171.
Gütlich, P., Gaspar, A. B. & Garcia, Y. (2013). *Beilstein J. Org. Chem.* **9**, 342–391.
Gütlich, P. & Goodwin, H. A. (2004a). Editors. *Spin-Crossover in Transition Metal Compounds*, Vols. I–III, *Topics in Current Chemistry.* Berlin: Springer.
Gütlich, P. & Goodwin, H. A. (2004b). *Top. Curr. Chem.* **233**, 1–48.
Gutlich, P., Ksenofontov, V. & Gaspar, A. B. (2005). *Coord. Chem. Rev.* **249**, 1811–1829.
Hauser, A. (2004). *Top. Curr. Chem.* **233**, 49–58.
Jeftić, J. & Hauser, A. (1997). *J. Phys. Chem. B*, **101**, 10262–10270.
Jeftić, J., Hinek, R., Capelli, S. C. & Hauser, A. (1997). *Inorg. Chem.* **36**, 3080–3087.
Jeftić, J., Romstedt, H. & Hauser, A. (1996). *J. Phys. Chem. Solids*, **57**, 1743–1750.
Kitazawa, T., Gomi, Y., Takahashi, M., Takeda, M., Enomoto, M., Miyazaki, A. & Enoki, T. (1996). *J. Mater. Chem.* **6**, 119–121.
Klotz, S. (2012). *Techniques in High Pressure Neutron Scattering*, pp. 69–74. Boca Raton: CRC Press.
Ksenofontov, V., Gaspar, A. B. & Gütlich, P. (2004). *Top. Curr. Chem.* **235**, 23–64.
Legrand, V., Le Gac, F., Guionneau, P. & Létard, J.-F. (2008). *J. Appl. Cryst.* **41**, 637–640.
Legrand, V., Pechev, S., Létard, J. F. & Guionneau, P. (2013). *Phys. Chem. Chem. Phys.* **15**, 13872–13880.
Lehmann, M. S. & Larsen, F. K. (1974). *Acta Cryst.* A**30**, 580–584.
Lemée-Cailleau, M. H. E., Colivet, C., Ouladdiaf, B., Moussa, F., Jeftic, J. & Létard, J. (2007). *J. Magn. Magn. Mater.* **310**, 1792–1793.
Linert, W. & Verdaguer, M. (2003). Editors. *Molecular Magnets: Recent Highlights.* Vienna: Springer.
McIntyre, G. J., Lemée-Cailleau, M. H. & Wilkinson, C. (2006). *Physica B*, **385–386**, 1055–1058.

McIntyre, G. J., Mélési, L., Guthrie, M., Tulk, C. A., Xu, J. & Parise, J. B. (2005). *J. Phys. Condens. Matter*, **17**, s3017–S3024.

Molnár, G., Kitazawa, T., Dubrovinsky, L., McGarvey, J. J. & Bousseksou, A. (2004). *J. Phys. Condens. Matter*, **16**, S1129–S1136.

Molnár, G., Niel, V., Real, J. A., Dubrovinsky, L., Bousseksou, A. & McGarvey, J. J. (2003). *J. Phys. Chem. B*, **107**, 3149–3155.

Muñoz, M. C. & Real, J. A. (2011). *Coord. Chem. Rev.* **255**, 2068–2093.

Muñoz-Lara, F. J., Arcís-Castillo, Z., Muñoz, M. C., Rodríguez-Velamazán, J. A., Gaspar, A. B. & Real, J. A. (2012). *Inorg. Chem.* **51**, 11126–11132.

Nardelli, M. (1995). *J. Appl. Cryst.* **28**, 659.

Niel, V., Galet, A., Gaspar, A. B., Muñoz, M. C. & Real, J. A. (2003). *Chem. Commun.* pp. 1248–1249.

Niel, V., Martinez-Agudo, J. M., Muñoz, M. C., Gaspar, A. B. & Real, J. A. (2001). *Inorg. Chem.* **40**, 3838–3839.

Niel, V., Thompson, A. L., Goeta, A. E., Enachescu, C., Hauser, A., Galet, A., Muñoz, M. C. & Real, J. A. (2005). *Chem. Eur. J.* **11**, 2047–2060.

Niel, V., Thompson, A. L., Muñoz, M. C., Galet, A., Goeta, A. E. & Real, J. A. (2003). *Angew. Chem. Int. Ed.* **42**, 3760–3763.

Ohkoshi, S., Imoto, K., Tsunobuchi, Y., Takano, S. & Tokoro, H. (2011). *Nat. Chem.* **3**, 564–569.

Papanikolaou, D., Margadonna, S., Kosaka, W., Ohkoshi, S., Brunelli, M. & Prassides, K. (2006). *J. Am. Chem. Soc.* **128**, 8358–8363.

Rodríguez-Velamazán, J. A., Carbonera, C., Castro, M., Palacios, E., Kitazawa, T., Létard, J. F. & Burriel, R. (2010). *Chem. Eur. J.* **16**, 8785–8796.

Rodríguez-Velamazán, J. A., Castro, M., Palacios, E., Burriel, R., Kitazawa, T. & Kawasaki, T. (2007). *J. Phys. Chem. B*, **111**, 1256–1261.

Sheldrick, G. M. (2008). *Acta Cryst.* A**64**, 112–122.

Shepherd, H. J., Bartual-Murgui, C., Molnár, G., Real, J. A., Muñoz, M. C., Salmon, L. & Bousseksou, A. (2011). *New J. Chem.* **35**, 1205–1210.

Shepherd, H. J., Bonnet, S., Guionneau, P., Bedoui, S., Garbarino, G., Nicolazzi, W., Bousseksou, A. & Molnár, G. (2011). *Phys. Rev. B*, **84**, 144107.

Shepherd, H. J., Palamarciuc, T., Rosa, P., Guionneau, P., Molnar, G., Létard, J.-F. & Bousseksou, A. (2012). *Angew. Chem. Int. Ed.* **51**, 3910–3914.

Shepherd, H. J., Rosa, P., Vendier, L., Casati, N., Létard, J.-F., Bousseksou, A., Guionneau, P. & Molnar, G. (2012). *Phys. Chem. Chem. Phys.* **14**, 5265–5271.

Slichter, C. P. & Drickamer, H. G. (1972). *J. Chem. Phys.* **56**, 2142–2160.

Spek, A. L. (2009). *Acta Cryst.* D**65**, 148–155.

Wilkinson, C., Cowan, J. A., Myles, D. A. A., Cipriani, F. & McIntyre, G. J. (2002). *Neutron News*, **13**, 37–41.

Wilkinson, C., Khamis, H. W., Stansfield, R. F. D. & McIntyre, G. J. (1988). *J. Appl. Cryst.* **21**, 471–478.